

[CLS] Attention is All You Need for Training-Free Visual Token Pruning: Make VLM Inference Faster

Qizhe Zhang^{1,2*} Aosong Cheng¹ Ming Lu³ Zhiyong Zhuo¹ Minqi Wang¹

Jiajun Cao¹ Shaobo Guo² Qi She² Shanghang Zhang^{1†}

¹ National Key Laboratory for Multimedia Information Processing,
School of Computer Science, Peking University

² ByteDance

³ Intel Labs China

Abstract

Large vision-language models (VLMs) often rely on a substantial number of visual tokens when interacting with large language models (LLMs), which has proven to be inefficient. Recent efforts have aimed to accelerate VLM inference by pruning visual tokens. Most existing methods assess the importance of visual tokens based on the text-visual cross-attentions in LLMs. In this study, we find that the cross-attentions between text and visual tokens in LLMs are inaccurate. Pruning tokens based on these inaccurate attentions leads to significant performance degradation, especially at high reduction ratios. To this end, we introduce **FasterVLM**, a simple yet effective training-free visual token pruning method that evaluates the importance of visual tokens more accurately by utilizing attentions between the [CLS] token and image tokens from the visual encoder. Since FasterVLM eliminates redundant visual tokens immediately after the visual encoder, ensuring they do not interact with LLMs and resulting in faster VLM inference. It is worth noting that, benefiting from the accuracy of [CLS] cross-attentions, FasterVLM can prune 95% of visual tokens while maintaining 90% of the performance of LLaVA-1.5-7B. We apply FasterVLM to various VLMs, including LLaVA-1.5, LLaVA-NeXT, and Video-LLaVA, to demonstrate its effectiveness. Experimental results show that our FasterVLM maintains strong performance across various VLM architectures and reduction ratios, significantly outperforming existing text-visual attention-based methods. Our code is available at <https://github.com/Theia-4869/FasterVLM>.

1 Introduction

With recent advances in large language models (LLMs) [3, 13, 38, 43, 44, 54, 55, 64], numerous efforts have been made to extend their powerful reasoning capabilities to multi-modal tasks [14, 35, 62], giving rise to vision language models (VLMs) such as GPT-4 [1], Gemini [51], LLaVA [34], and Qwen-VL [2]. These VLMs typically contain a visual encoder (*e.g.* CLIP) to convert visual inputs into sequential representations, and an LLM (*e.g.* Llama 2) for text generation, with modal alignment for the LLM to accept visual tokens as input [34]. Although these approaches have achieved remarkable performance in multi-modal tasks like visual question answering [15, 16, 20, 36, 50], the visual tokens, which comprise the majority of the input sequence, significantly increase the computational complexity and cost of VLM inference. Some work improves model performance by increasing input image resolution [33, 37, 59], but this leads to longer visual token sequences, further escalating computational overhead, which can be even worse in video models like Video-LLaVA [30].

*Work done during an internship at ByteDance.

†Corresponding author: shanghang@pku.edu.cn.

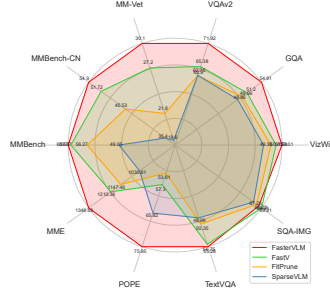


Figure 1: Comparison of LLaVA-1.5-7B on a range of **10** benchmarks, with a **90%** reduction ratio. **FasterVLM** outperforms other methods by a large margin on **9** tasks and achieves comparable results on the remaining one.

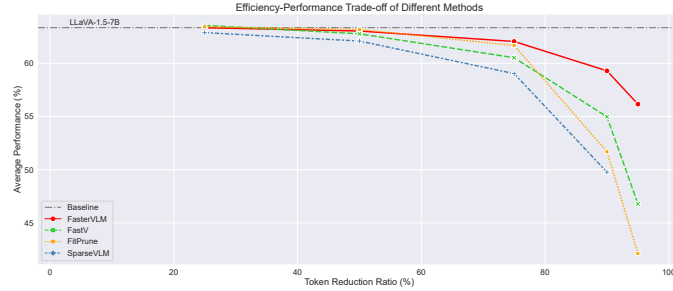


Figure 2: Relationship between performance and efficiency of different methods for LLaVA-1.5-7B. The *x*-axis stands for the reduction ratio of visual tokens, and the *y*-axis stands for the averaged performance of 10 benchmarks. While other methods suffer significant performance degradation as the token reduction ratio increases, **FasterVLM** maintains most performance (**90%** of vanilla LLaVA-1.5-7B) even at a high reduction ratio (**95%**).

To reduce the inference cost of VLMs, FastV [8] analyses the information flow in LLMs within VLMs and identifies the inefficient visual attention phenomenon: In the deeper layers of the LLM (after layer 2), visual tokens receive significantly less attention than their textual counterparts, implying that less useful information flows from visual tokens to the text portion, motivating the pruning of visual tokens in VLMs. According to the distribution of attention in different layers, FastV proposes an intuitive solution, ranking the visual tokens based on attention scores received after layer 2 of the LLM and pruning the lowest $R\%$ according to the computational budget, thereby reducing visual token redundancy and improving VLM inference efficiency. Subsequently, more work follows this paradigm [61, 65], utilizing various methods to prune visual tokens through text-visual attention from the LLM. Although FastV successfully identifies the inefficiency of visual tokens in VLMs, pruning based on text-visual attention is not effective. As shown in Fig. 2, the performance of VLM degrades significantly as the reduction ratio increases.

In this paper, we find that **the text-visual attention within the LLMs of current VLMs fails to align well with the actual significance of visual tokens, meaning that the attention weights assigned to each visual token do not correspond appropriately to their importance in the task**. This misalignment can be explained from two aspects, termed *attention shift* and *attention dispersion*. Specifically, *attention shift* refers to a tendency for textual attention to focus more on later parts of the visual token sequence, which is not desirable for preserving valuable visual information. We attribute this phenomenon to two main factors: the unidirectional information flow within the LLM and the relative positional relationships between tokens. These factors cause textual prompts to preferentially focus on the visual tokens positioned later in the sequence. Conversely, *Attention dispersion* refers to the less concentrated attention distribution within the LLM compared to the visual encoder. In the LLM, more visual tokens receive relatively high attention scores, but the highest attention value is lower. We believe that, despite the multi-modal projector’s role in aligning visual representations with text embeddings, a gap still remains between them. This gap results in noisy text-visual attention at shallower layers, hindering the effective pruning of important visual tokens.

To more accurately evaluate the importance of visual tokens, we introduce **FasterVLM**, a simple yet effective pruning method. FasterVLM directly utilizes the attention weights from the [CLS] token within the image encoder to assess the importance of each visual token. By removing tokens with lower attention scores before they are processed by the LLM, we achieve maximum inference acceleration. Quantitative and qualitative analyses indicate that [CLS] attention does not exhibit the shift phenomenon, thanks to the global attention mechanism in the image encoder. Moreover, **compared to text-visual attention, [CLS] attention is more concentrated, serving as a better indicator for evaluating the importance of visual tokens**. As noted in [11], certain artifacts exist in the attention maps of Vision Transformers [42, 45, 53], where the regions contain pixels highly similar to their surroundings. The model discards local information from these regions and stores global information in these artifacts. We find that these global tokens significantly impact VLM performance. Under high reduction ratios, previous methods struggle to identify these artifacts due to inaccurate text-visual attention. In contrast, FasterVLM can accurately identify these visual tokens containing global information via [CLS] attention, preserving most of the performance.

Benefiting from the simple design, FasterVLM can be easily applied to different VLMs, including LLaVA-1.5 [32], LLaVA-NeXT [33], and Video-LLaVA [30]. As shown in Fig. 2, extensive experiments on various vision-language benchmarks demonstrate that FasterVLM consistently outperforms other text-visual attention-based methods under different reduction ratios. For example, FasterVLM is capable of pruning 95% of visual tokens in LLaVA-1.5-7B, reducing inference FLOPs by more than 95%, and maintaining 90% of the original performance across 10 tasks without requiring any additional training (details for each task are provided in Fig. 1). In scenarios involving longer visual token sequences—such as high-resolution images (LLaVA-NeXT) or video inputs (Video-LLaVA)—FasterVLM continues to achieve superior performance with its simple design.

In summary, the contributions of our work are threefold:

1. We uncover that the inaccuracies of text-visual attention in the LLM—stemming from *attention shift* and *attention dispersion*—compromise its effectiveness for visual token pruning, and we provide a detailed explanation of these phenomena.
2. We introduce **FasterVLM**, a simple yet effective training-free visual token pruning method that evaluates the importance of visual tokens more accurately by the cross-attentions between the [CLS] token and image tokens from the visual encoder.
3. We apply FasterVLM to different types of VLMs and conduct extensive experiments on various vision-language tasks, showing that FasterVLM consistently outperforms existing methods and maintains high performance even under extreme reduction ratios.

2 Related Work

2.1 Vision-Language Models (VLMs)

The recent impressive success of large language models (LLMs) [3, 13, 38, 43, 44, 54, 55, 64] leads to a trend of extending their powerful reasoning capabilities to multi-modal comprehension tasks, giving birth to vision-language models (VLMs) [1, 51]. These VLMs generally include a visual encoder for serializing representations of input images and an LLM for text generation. To make the LLM acceptable for visual representations as input, VLMs typically align the visual and language modalities with an alignment module, which can be a simple linear layer [34], an MLP projector [32], or a deep query-based network [2, 26]. Although this allows the LLM to have visual perception, the introduction of long visual token sequences increases the computational burdens. Furthermore, studies have shown that existing VLMs still suffer from visual shortcomings [52] or hallucinations [18]. To mitigate this, efforts have been made to improve VLM performance by increasing the resolution of input images [37, 59], which further exacerbates the computation. For example, LLaVA-1.5 [34] encodes an image with 336 resolution into 576 visual tokens, while LLaVA-NeXT [33] doubles the resolution, resulting in 2880 tokens, potentially dozens of times more than the textual prompts. For video inputs, Video-LLaVA [30] needs to handle even more visual tokens from multiple frames, making VLM inference prohibitively expensive. Optimizing the inference process of VLMs is an urgent task to enable their application in resource-constrained real-world scenarios.

2.2 Token Compression for VLMs

One way to optimize VLM inference is by compressing the visual tokens that occupy the majority of the input sequence. Several studies have explored token sequence compression in language models [9, 19, 41, 46]. Compared with text, image information tends to have higher redundancy, making visual token compression for VLMs more reasonable and effective. LLaVA-PurMerge [48] leverages attention mechanisms to select important visual tokens and merges them using similar key clustering, achieving competitive performance while improving VLM inference efficiency. LLaVolta [7] proposes a heuristic and stage-wise compression method that reduces VLM training costs while largely maintaining original performance. TokenPacker [27] adopts a coarse-to-fine approach, using point-to-region attention to retain richer details while compressing visual tokens. MQT [17] and M³ [5] employ Matryoshka Representation Learning [25] to hierarchically compress visual tokens, reducing the number of tokens to no more than 10. However, these methods require additional training for VLMs to adapt to the compressed visual representations. In this work, we focus on VLM inference optimization without additional training.

2.3 Token Pruning for VLMs

Token pruning is another approach to improve model inference efficiency by removing less important tokens from the sequence. With the emergence of Transformer-based networks, this technique has been actively explored in natural language processing [22, 60] and computer vision [40, 47]. However, effective pruning of visual tokens in VLMs still remains under-explored. FastV [8] first identifies the redundancy and inefficiency of visual tokens in VLMs and proposed a simple method to remove visual tokens with low attention scores after the layer 2 of LLM. Subsequently, FitPrune [61] introduces a method to fit pruning recipes based on attention statistics, while SparseVLM [65] removes distractions from text prompts and uses more accurate text attention to progressively sparsify visual tokens. However, these approaches rely on text-visual attention within the LLM to evaluate the importance of visual tokens. In this work, we show that such attention does not align well with visual token importance and propose that pruning based solely on the [CLS] attention from the visual encoder yields unexpectedly good performances.

3 Inaccurate Text-Visual Attention in VLMs

Text-visual attention from the LLM Decoder in VLMs is often used to evaluate the importance of visual tokens for pruning. However, we find this attention does not align with the actual importance of visual tokens. To understand this misalignment, we first introduce the attention mechanism in the visual encoder and LLM decoder of VLMs in Sec. 3.1 as preliminaries. Then, in Sec. 3.2 and Sec. 3.3, we describe two phenomena observed in the visual attention of LLM decoder, termed *attention shift* and *attention dispersion*, corresponding to the position and intensity of attention respectively. These phenomena are absent in the visual encoder of VLMs, which motivates our use of [CLS] attention as a more reliable indicator of visual token importance.

3.1 Preliminaries

Existing VLMs typically consist of two core components: a visual encoder and an LLM decoder, both are the Transformer-based architecture [12, 56]. Although they both rely on the self-attention mechanism, there are subtle differences in specific implementations. In VLMs, the visual encoder (*e.g.* CLIP [45]) employs a global attention mechanism, where the patch-wise image $\mathbf{X} = [\mathbf{x}_{\text{cls}}; \mathbf{x}_{\text{img}}^1, \mathbf{x}_{\text{img}}^2, \dots, \mathbf{x}_{\text{img}}^n] \in \mathbb{R}^{(n+1) \times d}$ is first converted into the query \mathbf{Q} , key \mathbf{K} and value \mathbf{V} through three weight matrices $\mathbf{W}_Q, \mathbf{W}_K, \mathbf{W}_V \in \mathbb{R}^{d \times d}$ respectively:

$$\mathbf{Q} = \mathbf{X}\mathbf{W}_Q, \quad \mathbf{K} = \mathbf{X}\mathbf{W}_K, \quad \mathbf{V} = \mathbf{X}\mathbf{W}_V \quad (1)$$

where n is the length of the image token sequence, and d is the size of the hidden state. Then, the scaled dot-product attention is calculated as follows:

$$\mathbf{A} = \text{Softmax} \left(\frac{\mathbf{Q}\mathbf{K}^T}{\sqrt{d}} \right), \quad \mathbf{O} = \mathbf{A}\mathbf{V} \quad (2)$$

Here, we refer to the first row of \mathbf{A} as [CLS] attention.

While the LLM decoder utilizes causal self-attention [56], where each token can only attend to the previous tokens (*i.e.* those from the past) and not the following ones (*i.e.* those from the future). For the whole input sequence $\mathbf{X} = [\mathbf{x}_{\text{sys}}; \mathbf{x}_{\text{img}}; \mathbf{x}_{\text{txt}}; \mathbf{x}_{\text{out}}] \in \mathbb{R}^{l \times d}$, the query \mathbf{Q} , key \mathbf{K} and value \mathbf{V} are obtained in the same way, and the causal attention is then calculated as:

$$\mathbf{A} = \text{Softmax} \left(\frac{\mathbf{Q}\mathbf{K}^T + \mathbf{M}}{\sqrt{d}} \right), \quad \mathbf{O} = \mathbf{A}\mathbf{V} \quad (3)$$

where l is the total length of the input sequence (including system prompt, image patches, text question, and output answer), and $\mathbf{M} \in \mathbb{R}^{l \times l}$ is a lower triangular causal mask ensuring that each token attends only to itself and previous tokens. Our focus is on the attention received by visual tokens from three sources: *image attention* (from the image patches themselves), *text attention* (from the text prompt), and *last attention* (from the output answer since we only extract attention at the prefill phase, where the output contains only a single token). Multi-head attention is averaged across all heads following FastV [8] for analysis.

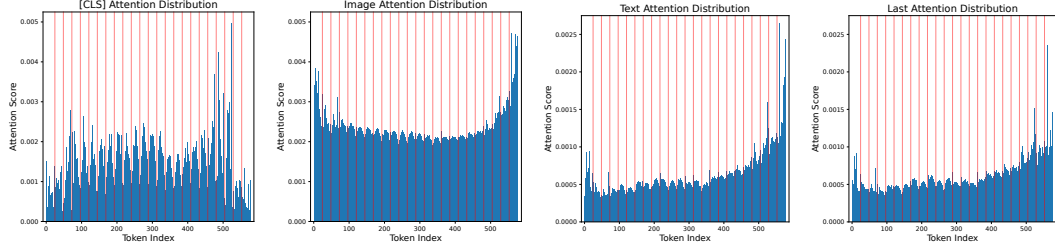


Figure 3: Distribution of attention received by visual tokens from different sources, arranged from left to right: [CLS] token, image patches, text prompt, and last token (for output generation). From attention distributions within the LLM decoder (image, text, and last), we observe an obvious trend where attention intensity gradually increases with token indices, a phenomenon we term *attention shift*. Notably, the same trend does not show up in [CLS] attention.

3.2 Text-Visual Attention Shift

To analyze text-visual attention in VLMs, we first randomly sample N image-text pairs from the LLaVA-mix665k data [32]. These samples are then used to prompt the VLM to generate responses, during which we extract the attention received by the visual tokens. In this section, N is set to 1,000, and we use LLaVA-1.5-7B as the VLM, following the original configuration in [32]. We analyze the distribution of attention scores with respect to token indices, with sources including the [CLS] token from the visual encoder, as well as image patches, text prompt, and output response from the LLM decoder (after layer 2, following [8]).

As shown in Fig. 3, a clear trend is visible across all attention distributions within the LLM decoder (image, text, and last), where attention scores increase with larger token indices. This suggests that if visual tokens were pruned based on text-visual attention from the LLM decoder, most retained visual tokens would be located in the lower half of the input image, potentially leading to a serious loss of important visual information. We attribute this phenomenon to the unidirectional nature of attention in the LLM, as this trend does not appear in the visual encoder, which employs global attention. Although this causal attention is the core of the next-token prediction paradigm, it is not well-suited for assessing the importance of visual tokens. As shown in the distribution plots, attention from the [CLS] token serves as a more reliable indicator for token pruning. In addition, the red vertical lines in Fig. 3 denote the length of each row in the input image (24 for CLIP-ViT-L-14-336px in LLaVA-1.5). Compared to the attention in the LLM decoder, [CLS] attention is more sensitive to image boundary areas, allocating more attention to central regions containing richer information, which further supports its effectiveness for evaluating visual token importance.

3.3 Text-Visual Attention Dispersion

In addition to the attention location distribution, we also analyze the distribution of attention intensity to further illustrate the lack of concentration in text-visual attention. The concentration here implies that a small number of tokens receive the majority of attention, while most tokens have low attention scores, indicating that the model identifies important tokens with high certainty. In row 1 of Fig. 4, we visualize the attention of the [CLS] token and the last output token on the visual tokens within the same image. It is apparent that [CLS] attention is highly focused, with only a few tokens receiving significant attention distributed in different positions like the aircraft nose, tail, runway, and sky. These tokens capture global information about the input image, and retaining them can accelerate VLM inference while preserving most of the performance. In contrast, the last output token attention (as well as other text tokens) is more dispersed, with multiple regions across the image receiving high attention, making it challenging to select important visual tokens during pruning. It is worth noting that in the last attention map, tokens with high attention in the [CLS] attention map receive little attention, while tokens with high attention scores are concentrated in the lower part of the image, including areas like the runway, grass, and even padding, which contain little valuable information. This aligns with the *attention drift* phenomenon discussed in the previous section.

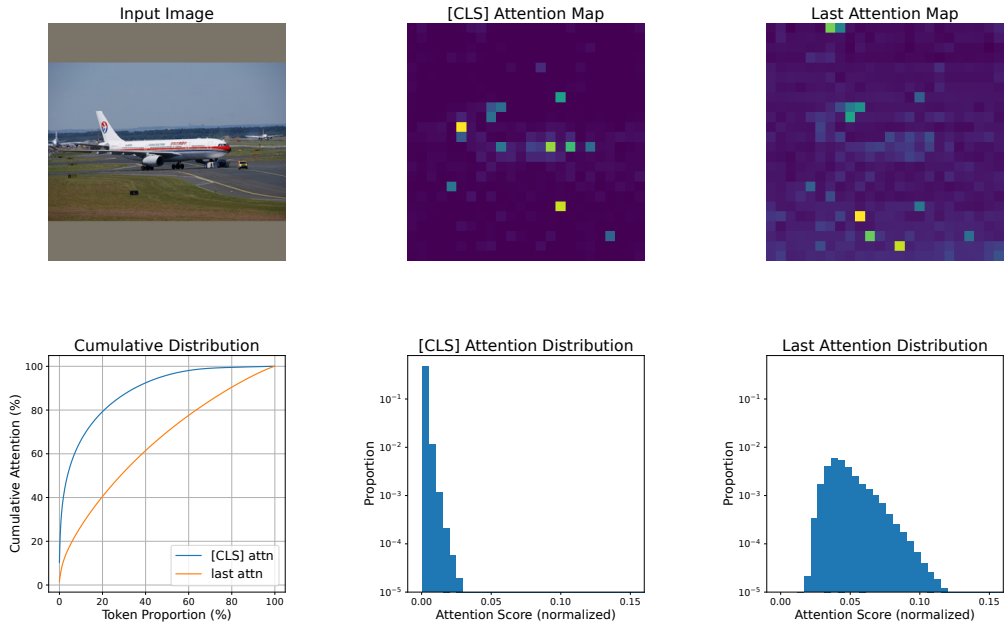


Figure 4: Concentration of [CLS] attention and last attention. The first row displays the input image and maps of [CLS] and the last attentions received by corresponding regions. The second row shows the CDF and the intensity distribution of [CLS] and the last attention. From multiple perspectives, it is evident that [CLS] attention is more concentrated than last attention.

In row 2 of Fig. 4, we first compute the Cumulative Distribution Function (CDF) of attention scores for visual tokens sorted by their attention scores, as shown in the left sub-figure. The CDF curve of [CLS] attention is significantly steeper than that of last attention, indicating that [CLS] attention is more concentrated. In the [CLS] attention distribution, the top 20% of visual tokens receive about 80% of total attention, compared to over 60% for last attention. In the remaining two sub-figures, we respectively show the average distribution of [CLS] and last attention intensity across N samples. Most visual tokens receive minimal [CLS] attention, while last attention is more uniformly distributed, which means it contains more noise. The lack of *attention dispersion* in [CLS] attention suggests it is a more suitable indicator for guiding visual token pruning.

4 [CLS] Attention for Visual Token Pruning

Based on the above analysis of attention in VLMs, we propose FasterVLM, which uses [CLS] attention from the visual encoder as a more accurate indicator for visual token pruning. By removing redundant visual tokens before the LLM decoder, our approach could make VLM inference faster than methods that prune tokens within the LLM.

4.1 FasterVLM

To achieve more accurate visual token pruning, we propose FasterVLM, which leverages [CLS] attention from the visual encoder to rerank visual tokens and filter out the lower parts. Fig. 5 illustrates our FasterVLM design. At the output layer of the visual encoder (*e.g.* the penultimate layer of CLIP [45] in LLaVA-1.5 [32]), the attention from the [CLS] token $z_{[CLS]} \in \mathbb{R}^d$ to other image tokens $Z_v \in \mathbb{R}^{n \times d}$ is computed by:

$$q_{[CLS]} = z_{[CLS]} W_Q, \quad K_v = Z_v W_V, \quad a_{[CLS]} = \text{Softmax} \left(\frac{q_{[CLS]} K_v^T}{\sqrt{d}} \right) \quad (4)$$

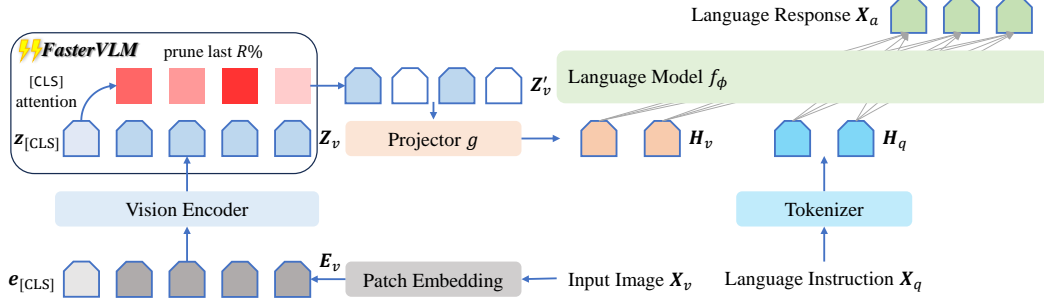


Figure 5: Illustration of **FasterVLM**. We first re-rank image tokens using [CLS] attention from the visual encoder and prune the last $R\%$. The remaining image tokens, after passing through the multi-modal projector, are combined with language instructions as input to the language model for response generation. Since redundant image tokens are removed before the language model, FasterVLM can make the inference of the entire VLM even faster than pruning within the language model.

where n is the length of image tokens, d is the size of hidden states, and $\mathbf{W}_Q, \mathbf{W}_V$ is the transformation matrices for queries and keys at this layer. Using this [CLS] attention, we derive a dynamic threshold based on the computation budget R :

$$\tau = \min \{ \tau \mid |\{a \in \mathbf{a}_{[\text{CLS}]} \mid a \geq \tau\}| \leq n \times (1 - R) \} \quad (5)$$

In practice, τ is set as the $(1 - R)$ percentile of $\mathbf{a}_{[\text{CLS}]}$. With this threshold, we can prune unimportant tokens by:

$$\mathbf{Z}'_v = \{\mathbf{z}'_v \in \mathbf{Z}_v \mid \mathbf{a}_{[\text{CLS}]}^i \geq \tau\} \quad (6)$$

The remaining image tokens, after passing through a multi-modal projector g , are concatenated with language instructions \mathbf{H}_q and fed into the language model f_ϕ to generate the response \mathbf{X}_a :

$$\mathbf{X}_a = f_\phi([g(\mathbf{Z}'_v); \mathbf{H}_q]) \quad (7)$$

Here, $[\cdot; \cdot]$ denotes the concatenate operation. By performing token pruning before the LLM decoder, we dynamically adjust the number of visual tokens as input to the language model based on the actual computational budget, thus accelerating the VLM inference.

4.2 Theoretical Computation Reduction

Since the length of language instructions is uncertain and typically much shorter than the length of visual tokens, we only consider the FLOPs associated with visual tokens. In the language model of the VLM, assume n is the number of visual tokens, d is the hidden state size and m is the intermediate size of FFN (with SwiGLU [49] activation in LLaMA [54]). For the prefill stage, the FLOPs of a single transformer layer can be estimated by $8nd^2 + 4n^2d + 6ndm$, and the theoretical FLOPs reduction with a token reduction ratio R (and $\hat{n} = (1 - R) \cdot n$) is calculated as:

$$F = 1 - \frac{8\hat{n}d^2 + 4\hat{n}^2d + 6\hat{n}dm}{8nd^2 + 4n^2d + 6ndm} = R + \frac{2n}{4d + 2n + 3m}(R - R^2) \quad (8)$$

Since the second term is relatively small, the overall FLOP reduction is close to R but slightly higher. In the decode stage with KV cache, the attention complexity reduces to $\mathcal{O}(n)$, and the FLOPs for a transformer layer can be re-estimated by $8d^2 + 4nd + 6ndm$. In this case, the theoretical FLOPs reduction is still close to R but slightly lower. Moreover, existing hardware does not adapt well to the varying KV cache length during inference, so pruning before the LLM decoder (our FasterVLM implementation) actually results in more inference acceleration.

5 Experiments

In this section, we validate our method across various VLM architectures on comprehensive multi-modal benchmarks, including high-resolution image and video understanding tasks. We compare our approach with multiple existing methods and conduct an efficiency analysis.

Table 1: Performance comparison of different methods with LLaVA-1.5-7B across 10 benchmarks at reduction ratios ranging from 50% to 95%. For each reduction ratio, the best average performance is shown in **bold**. Our **FasterVLM** consistently achieves the best performance across all reduction ratios. Notably, even with 95% of visual tokens pruned, our method maintains **89.41%** performance, demonstrating its effectiveness in accurately identifying the most critical visual information.

Method	Reduction Ratio	# Token	VQAv2	GQA	VizWiz	SQA-IMG	TextVQA	POPE	MME	MMB	MMB-CN	MM-Vet	Average
LLaVA-1.5-7B	0%	576	78.52	61.94	50.06	69.51	58.21	85.88	1506.47	64.69	58.08	31.30	100.00%
FastV FitPrune SparseVLM FasterVLM	50%	288	77.67	60.05	50.53	68.96	58.25	82.45	1513.06	64.26	58.16	31.70	99.33%
			78.41	61.70	50.04	69.16	58.26	85.37	1499.70	64.60	58.16	31.10	99.73%
			76.67	58.78	51.03	68.57	57.49	83.87	1458.79	63.14	56.87	31.50	98.52%
			77.86	60.64	50.45	68.37	57.90	86.20	1471.96	63.83	56.70	34.80	100.12%
FastV FitPrune SparseVLM FasterVLM	75%	144	74.07	56.58	51.29	69.11	57.38	73.74	1463.39	64.00	57.22	28.60	95.80%
			76.14	59.38	51.30	69.01	56.49	80.75	1472.86	63.92	57.65	28.40	97.22%
			72.76	55.11	51.46	69.36	55.99	77.57	1351.65	59.54	51.03	29.90	93.84%
			76.19	58.34	51.97	67.92	57.07	83.46	1433.76	62.54	57.13	34.20	98.75%
FastV FitPrune SparseVLM FasterVLM	90%	58	65.38	51.20	51.84	69.81	54.75	57.30	1210.36	59.97	51.72	27.20	87.97%
			62.76	49.96	50.85	68.22	50.35	53.81	1147.46	56.27	45.53	21.80	82.07%
			62.90	48.86	49.36	67.23	48.99	65.82	1030.61	49.05	35.40	18.60	78.13%
			71.92	54.91	53.01	68.91	55.28	75.85	1348.63	60.57	54.90	30.10	94.24%
FastV FitPrune FasterVLM	95%	29	55.92	46.03	49.10	70.00	51.56	35.47	971.56	50.17	42.18	18.90	74.93%
			52.39	43.60	48.61	68.32	46.75	31.17	855.21	39.69	29.98	18.00	67.64%
			66.75	51.51	52.67	69.56	53.09	67.24	1254.80	58.51	51.98	27.50	89.41%

5.1 Experimental Setup

Datasets. We conduct extensive experiments on 10 image-based multi-modal benchmarks, including common visual question answering tasks such as VQAv2 [15], GQA [20], VizWiz [16], ScienceQA-IMG [36], and TextVQA [50], as well as other multi-modal benchmarks such as POPE [29], MME [14], MMBench [35], MMBench-CN [35] and MM-Vet [62]. Additionally, we also experiment on 4 widely used video question answering benchmarks, including TGIF-QA [21], MSVD-QA [57], MSRVTT-QA [57], and ActivityNet-QA [63]. All experiments on these benchmarks follow the default settings and evaluation metrics. Details of each task are provided in the appendix.

Model architectures. We apply FasterVLM to various VLM architectures, including the classic LLaVA-1.5 [32] models with both 7B and 13B parameters, LLaVA-NeXT-7B [33] for high-resolution image inputs, and Video-LLaVA-7B [30] for video understanding. For all models, we follow the same inference settings as the original papers.

Comparison methods. We choose FastV [8], FitPrune [61], and SparseVLM [65] as comparison methods. All methods rely on text-visual attention in the LLM decoder for visual token pruning without additional training. FastV, as the initial approach, performs a one-time pruning after the second layer in the LLM. FitPrune derives an optimal pruning strategy based on predefined computational budgets, gradually pruning at each layer. SparseVLM, on the other hand, pre-selects text prompts used to guide pruning, aiming to reduce noise in text-visual attention.

5.2 Main results

We first apply FasterVLM to the widely used LLaVA-1.5 model and conduct a comprehensive comparison with existing methods. Tab. 1 shows the performance on the LLaVA-1.5-7B model as the visual token reduction ratio increases from 50% to 95%. We also plot the relationship between average performance and the visual token reduction ratio in Fig. 2. Note that SparseVLM includes a visual token recycling mechanism, which prevents reducing the visual token count below 95%. The results indicate that for all text-visual attention-based methods, model performance degrades noticeably as the reduction ratio increases, suggesting that text-based attention is not reliable in identifying the most important visual tokens. In contrast, our FasterVLM significantly mitigates this performance decline, retaining 89.41% of the original performance at a high reduction ratio of 95%, while substantially enhancing computational efficiency. This demonstrates the critical importance of [CLS] attention for effective visual token pruning.

We also validate our FasterVLM on the 13B version of LLaVA-1.5, with results shown in Tab. 2. Due to space constraints, we report only the average results across the 10 benchmarks. Detailed results can be found in the appendix. With a larger language model, the VLM achieves better performance on vision-language tasks, even with the same visual encoder. However, as the token pruning ratio increases, pruning methods based on text attention exhibit a similar, sharp decline in

Table 2: Performance comparison of different methods with LLaVA-1.5-13B under different reduction ratios, with results reported as the average of 10 benchmarks. For each reduction ratio, the best average performance is shown in **bold**.

Method	Reduction Ratio	# Token	Benchmark Average
LLaVA-1.5-13B	0%	576	100.00%
FastV			97.16%
SparseVLM	75%	144	94.32%
FasterVLM			97.43%
FastV			90.26%
SparseVLM	90%	58	85.02%
FasterVLM			93.68%
FastV			80.53%
FasterVLM	95%	29	88.35%

Table 3: Performance comparison of different methods with LLaVA-NeXT under different reduction ratios, with results reported as the average of 10 benchmarks. For each reduction ratio, the best average performance is shown in **bold**.

Method	Reduction Ratio	# Token	Benchmark Average
LLaVA-NeXT-7B	0%	2880	100.00%
FastV			97.37%
SparseVLM	75%	720	94.95%
FasterVLM			98.73%
FastV			89.24%
SparseVLM	90%	290	88.65%
FasterVLM			93.55%
FastV			77.43%
FasterVLM	95%	145	88.85%

Table 4: Video understanding performance with Video-LLaVA across 4 commonly used video question answering benchmarks at reduction ratios ranging from 75% to 95%. The best average performance at each reduction ratio is shown in **bold**. Performance is evaluated using the first 1,000 samples from each benchmark and *gpt-3.5-turbo* is used for scoring.

Method	Reduction Ratio	# Token	TGIF-QA		MSVD-QA		MSRVTT-QA		ActivityNet-QA		Average	
			Acc.	Score	Acc.	Score	Acc.	Score	Acc.	Score	Acc.	Score
Video-LLaVA	0%	2048	19.80	2.53	70.50	3.93	57.50	3.50	43.60	3.81	100.00%	100.00%
FastV			19.40	2.51	69.10	3.91	54.60	3.43	41.50	3.80	96.53%	99.12%
FasterVLM	75%	512	17.90	2.48	70.20	3.95	56.60	3.50	44.70	3.86	97.73%	99.88%
FastV			13.80	2.40	68.80	3.90	52.90	3.40	41.30	3.79	88.50%	97.63%
FasterVLM	90%	208	15.60	2.39	69.10	3.92	55.30	3.43	44.50	3.82	93.76%	98.04%
FastV			10.60	2.29	64.10	3.78	52.40	3.39	40.30	3.78	82.00%	95.64%
FasterVLM	95%	104	14.00	2.34	65.30	3.79	53.80	3.40	43.70	3.79	89.28%	96.37%

performance. In contrast, our method retains 88.35% of the original performance at a 95% reduction ratio, demonstrating that it achieves outstanding performance even with a larger language model.

5.3 FasterVLM with higher resolution

Some works [33, 37, 59] attempt to improve VLM performance on visual question answering tasks by increasing the input image resolution. However, this resolution increase introduces more visual tokens, further intensifying the computational load on the VLM. In this section, we apply FasterVLM to LLaVA-NeXT-7B, which can handle up to 2880 visual tokens. The results are presented in Tab. 3. Compared to LLaVA-1.5, LLaVA-NeXT involves a greater number of visual tokens, implying a higher degree of redundancy. At a 95% reduction ratio, retaining only 145 visual tokens, FasterVLM preserves 88.35% of the original performance, significantly outperforming FastV and FitPrune. This demonstrates the value of FasterVLM for high-resolution visual inputs.

5.4 FasterVLM with video understanding

In addition to high-resolution images, video is another scenario with high redundancy in visual tokens. Thanks to its simple design, we can easily apply FasterVLM to Video-LLaVA, which accepts videos as input. Following [39] and [30], we conduct experiments on four video question answering benchmarks, using ChatGPT-Assistant for evaluation. Due to the commercial API usage limits, we follow [8] to use the first 1K samples from each benchmark in our experiments. The evaluation results are shown in Tab. 4. Video-LLaVA processes 8 frames of 224-resolution video, totaling 2048 visual tokens. FasterVLM maintains 93.76% of the original performance at a 90% reduction ratio (retaining 130 tokens) and 89.28% with only 65 tokens (95% reduction ratio), significantly outperforming FastV. This improvement is due to the higher redundancy in temporally continuous video frames compared to single images, and the [CLS] attention accurately identifies key tokens within the video sequence, enabling FasterVLM to maintain strong performance even at high reduction ratios.

Table 5: Ablation studies of different pruning strategies on 3 benchmarks.

Pruning Strategy	TextVQA	POPE	MME
LLaVA-1.5-7B	58.21	85.88	1506.47
(a) w/ randomly prune 90% before LLM	48.45	74.77	1227.07
(b) w/ prune 90% by patch attn before LLM	54.15	70.39	1278.05
(c) w/ prune 90% by [CLS] attn before LLM	55.28	75.85	1348.63
(d) w/ prune 90% by [CLS] attn at LLM layer 2	55.18	73.51	1338.43
(e) w/ prune 90% by [CLS] attn and merge	49.72	68.19	1207.31

Table 6: Inference efficiency comparison between FastV and FasterVLM with LLaVA-NeXT.

Method	Reduction	# Token	FLOPs (T)	Storage (MB)	GPU Memory (GB)	Throughput (it/s)
LLaVA-NeXT-7B	0%	2880	41.65	1440	17.93	2.40
FastV	50%	1440	21.11	765	17.98	3.22
FasterVLM			19.74	720	16.23	3.48
FastV	95%	145	6.14	225	17.98	4.56
FasterVLM			3.77	144	15.28	5.25

5.5 Ablation study

Although our design is simple, it is both effective and efficient. To demonstrate this, we conduct a thorough ablation study on different strategies, presented in Tab. 5. Lines (a)-(c) examine different criteria for pruning visual tokens before the LLM, including random pruning (a), pruning based on the average self-attention among all image patches (b), and pruning based on [CLS] attention (c, used in our FasterVLM). Using image patch attention is less effective than [CLS] attention, as the [CLS] token contains more global information. Interestingly, random pruning does not perform poorly, further highlighting the redundancy of visual tokens in VLMs. In line (d), we prune tokens at the same layer as FastV but determine token importance based on [CLS] attention. This approach performs similarly to pruning before the LLM but results in lower inference efficiency. In line (e), we apply a commonly used strategy in token compression for VLMs, token merging, where each retained token is combined with its k most similar tokens based on key similarity after selecting important tokens using [CLS] attention. Unfortunately, this strategy proves unsuitable for training-free token pruning, as greater merging led to significant performance degradation. Thus, FasterVLM adopts the simplest yet most effective method, directly pruning visual tokens before the LLM using [CLS] attention.

5.6 Efficiency analysis

To demonstrate the efficiency of our FasterVLM, we perform a comparative analysis of FLOPs, cache storage, CUDA memory, and inference throughput with FastV on LLaVA-NeXT-7B. To get rid of the impact of output sequence length on the decoding time, we choose the SQA-IMG benchmark for analysis, where the model only outputs a single option. All experiments are performed on a single NVIDIA A100-80GB GPU. As shown in Tab. 6, at a 95% reduction ratio, FasterVLM achieves a $\times 2.2$ increase in throughput for LLaVA-NeXT. Compared to FastV with the same reduction ratio, FasterVLM requires less memory and achieves faster inference. This is because pruning within the LLM results in varying KV cache lengths, which is incompatible with current hardware. Moreover, the design of pruning before LLM enables compatibility with faster attention implementations like FlashAttention [10], which are infeasible for methods like FastV that require access to internal LLM attention information. Additional experiments are provided in the appendix.

6 Conclusion

In conclusion, we first reveal the inaccuracies in recent popular text-visual attention of VLMs for visual token pruning caused by the phenomena of *attention shift* and *attention dispersion*. Then, we introduce a straightforward and effective training-free visual token pruning method called FasterVLM, which evaluates the importance of visual tokens more accurately by the attentions between the [CLS] and image tokens from the visual encoder. By pruning the visual tokens before the LLM, we achieve better performance and faster inference than existing text-visual attention-based pruning methods.

References

- [1] Josh Achiam, Steven Adler, Sandhini Agarwal, Lama Ahmad, Ilge Akkaya, Florencia Leoni Aleman, Diogo Almeida, Janko Altenschmidt, Sam Altman, Shyamal Anadkat, et al. Gpt-4 technical report. *arXiv preprint arXiv:2303.08774*, 2023.
- [2] Jinze Bai, Shuai Bai, Shusheng Yang, Shijie Wang, Sinan Tan, Peng Wang, Junyang Lin, Chang Zhou, and Jingren Zhou. Qwen-vl: A frontier large vision-language model with versatile abilities. *arXiv preprint arXiv:2308.12966*, 2023.
- [3] Tom B Brown. Language models are few-shot learners. *arXiv preprint arXiv:2005.14165*, 2020.
- [4] Fabian Caba Heilbron, Victor Escorcia, Bernard Ghanem, and Juan Carlos Niebles. Activitynet: A large-scale video benchmark for human activity understanding. In *Proceedings of the ieee conference on computer vision and pattern recognition*, pages 961–970, 2015.
- [5] Mu Cai, Jianwei Yang, Jianfeng Gao, and Yong Jae Lee. Matryoshka multimodal models. *arXiv preprint arXiv:2405.17430*, 2024.
- [6] David Chen and William B Dolan. Collecting highly parallel data for paraphrase evaluation. In *Proceedings of the 49th annual meeting of the association for computational linguistics: human language technologies*, pages 190–200, 2011.
- [7] Jieneng Chen, Luoxin Ye, Ju He, Zhao-Yang Wang, Daniel Khashabi, and Alan Yuille. Llavorla: Efficient multi-modal models via stage-wise visual context compression. *arXiv preprint arXiv:2406.20092*, 2024.
- [8] Liang Chen, Haozhe Zhao, Tianyu Liu, Shuai Bai, Junyang Lin, Chang Zhou, and Baobao Chang. An image is worth 1/2 tokens after layer 2: Plug-and-play inference acceleration for large vision-language models. *arXiv preprint arXiv:2403.06764*, 2024.
- [9] Zihang Dai, Guokun Lai, Yiming Yang, and Quoc Le. Funnel-transformer: Filtering out sequential redundancy for efficient language processing. *Advances in neural information processing systems*, 33:4271–4282, 2020.
- [10] Tri Dao, Dan Fu, Stefano Ermon, Atri Rudra, and Christopher Ré. Flashattention: Fast and memory-efficient exact attention with io-awareness. *Advances in Neural Information Processing Systems*, 35:16344–16359, 2022.
- [11] Timothée Darcet, Maxime Oquab, Julien Mairal, and Piotr Bojanowski. Vision transformers need registers. *arXiv preprint arXiv:2309.16588*, 2023.
- [12] Alexey Dosovitskiy. An image is worth 16x16 words: Transformers for image recognition at scale. *arXiv preprint arXiv:2010.11929*, 2020.
- [13] Abhimanyu Dubey, Abhinav Jauhri, Abhinav Pandey, Abhishek Kadian, Ahmad Al-Dahle, Aiesha Letman, Akhil Mathur, Alan Schelten, Amy Yang, Angela Fan, et al. The llama 3 herd of models. *arXiv preprint arXiv:2407.21783*, 2024.
- [14] Chaoyou Fu, Peixian Chen, Yunhang Shen, Yulei Qin, Mengdan Zhang, Xu Lin, Jinrui Yang, Xiawu Zheng, Ke Li, Xing Sun, Yunsheng Wu, and Rongrong Ji. Mme: A comprehensive evaluation benchmark for multimodal large language models, 2024.
- [15] Yash Goyal, Tejas Khot, Douglas Summers-Stay, Dhruv Batra, and Devi Parikh. Making the v in vqa matter: Elevating the role of image understanding in visual question answering. In *Proceedings of the IEEE conference on computer vision and pattern recognition*, pages 6904–6913, 2017.
- [16] Danna Gurari, Qing Li, Abigale J Stangl, Anhong Guo, Chi Lin, Kristen Grauman, Jiebo Luo, and Jeffrey P Bigham. Vizwiz grand challenge: Answering visual questions from blind people. In *Proceedings of the IEEE conference on computer vision and pattern recognition*, pages 3608–3617, 2018.
- [17] Wenbo Hu, Zi-Yi Dou, Liunian Harold Li, Amita Kamath, Nanyun Peng, and Kai-Wei Chang. Matryoshka query transformer for large vision-language models. *arXiv preprint arXiv:2405.19315*, 2024.
- [18] Qidong Huang, Xiaoyi Dong, Pan Zhang, Bin Wang, Conghui He, Jiaqi Wang, Dahua Lin, Weiming Zhang, and Nenghai Yu. Opera: Alleviating hallucination in multi-modal large language models via over-trust penalty and retrospection-allocation. In *Proceedings of the IEEE/CVF Conference on Computer Vision and Pattern Recognition*, pages 13418–13427, 2024.
- [19] Xin Huang, Ashish Khetan, Rene Bidart, and Zohar Karnin. Pyramid-bert: Reducing complexity via successive core-set based token selection. *arXiv preprint arXiv:2203.14380*, 2022.
- [20] Drew A Hudson and Christopher D Manning. Gqa: A new dataset for real-world visual reasoning and compositional question answering. In *Proceedings of the IEEE/CVF conference on computer vision and pattern recognition*, pages 6700–6709, 2019.

[21] Yunseok Jang, Yale Song, Youngjae Yu, Youngjin Kim, and Gunhee Kim. Tgif-qa: Toward spatio-temporal reasoning in visual question answering. In *Proceedings of the IEEE conference on computer vision and pattern recognition*, pages 2758–2766, 2017.

[22] Sehoon Kim, Sheng Shen, David Thorsley, Amir Gholami, Woosuk Kwon, Joseph Hassoun, and Kurt Keutzer. Learned token pruning for transformers. In *Proceedings of the 28th ACM SIGKDD Conference on Knowledge Discovery and Data Mining*, pages 784–794, 2022.

[23] Ivan Krasin, Tom Duerig, Neil Alldrin, Vittorio Ferrari, Sami Abu-El-Haija, Alina Kuznetsova, Hassan Rom, Jasper Uijlings, Stefan Popov, Andreas Veit, et al. Openimages: A public dataset for large-scale multi-label and multi-class image classification. *Dataset available from https://github.com/openimages*, 2017.

[24] Ranjay Krishna, Yuke Zhu, Oliver Groth, Justin Johnson, Kenji Hata, Joshua Kravitz, Stephanie Chen, Yannis Kalantidis, Li-Jia Li, David A Shamma, et al. Visual genome: Connecting language and vision using crowdsourced dense image annotations. *International journal of computer vision*, 123:32–73, 2017.

[25] Aditya Kusupati, Gantavya Bhatt, Aniket Rege, Matthew Wallingford, Aditya Sinha, Vivek Ramanujan, William Howard-Snyder, Kaifeng Chen, Sham Kakade, Prateek Jain, et al. Matryoshka representation learning. *Advances in Neural Information Processing Systems*, 35: 30233–30249, 2022.

[26] Junnan Li, Dongxu Li, Silvio Savarese, and Steven Hoi. Blip-2: Bootstrapping language-image pre-training with frozen image encoders and large language models. In *International conference on machine learning*, pages 19730–19742. PMLR, 2023.

[27] Wentong Li, Yuqian Yuan, Jian Liu, Dongqi Tang, Song Wang, Jianke Zhu, and Lei Zhang. Tokenpacker: Efficient visual projector for multimodal llm. *arXiv preprint arXiv:2407.02392*, 2024.

[28] Yuncheng Li, Yale Song, Liangliang Cao, Joel Tetreault, Larry Goldberg, Alejandro Jaimes, and Jiebo Luo. Tgif: A new dataset and benchmark on animated gif description. In *Proceedings of the IEEE Conference on Computer Vision and Pattern Recognition*, pages 4641–4650, 2016.

[29] Yifan Li, Yifan Du, Kun Zhou, Jinpeng Wang, Wayne Xin Zhao, and Ji-Rong Wen. Evaluating object hallucination in large vision-language models. *arXiv preprint arXiv:2305.10355*, 2023.

[30] Bin Lin, Yang Ye, Bin Zhu, Jiaxi Cui, Munan Ning, Peng Jin, and Li Yuan. Video-llava: Learning united visual representation by alignment before projection. *arXiv preprint arXiv:2311.10122*, 2023.

[31] Tsung-Yi Lin, Michael Maire, Serge Belongie, James Hays, Pietro Perona, Deva Ramanan, Piotr Dollár, and C Lawrence Zitnick. Microsoft coco: Common objects in context. In *Computer Vision–ECCV 2014: 13th European Conference, Zurich, Switzerland, September 6–12, 2014, Proceedings, Part V 13*, pages 740–755. Springer, 2014.

[32] Haotian Liu, Chunyuan Li, Yuheng Li, and Yong Jae Lee. Improved baselines with visual instruction tuning. In *Proceedings of the IEEE/CVF Conference on Computer Vision and Pattern Recognition*, pages 26296–26306, 2024.

[33] Haotian Liu, Chunyuan Li, Yuheng Li, Bo Li, Yuanhan Zhang, Sheng Shen, and Yong Jae Lee. Llava-next: Improved reasoning, ocr, and world knowledge, 2024.

[34] Haotian Liu, Chunyuan Li, Qingyang Wu, and Yong Jae Lee. Visual instruction tuning. *Advances in neural information processing systems*, 36, 2024.

[35] Yuan Liu, Haodong Duan, Yuanhan Zhang, Bo Li, Songyang Zhang, Wangbo Zhao, Yike Yuan, Jiaqi Wang, Conghui He, Ziwei Liu, et al. Mmbench: Is your multi-modal model an all-around player? In *European Conference on Computer Vision*, pages 216–233. Springer, 2025.

[36] Pan Lu, Swaroop Mishra, Tanglin Xia, Liang Qiu, Kai-Wei Chang, Song-Chun Zhu, Oyvind Tafjord, Peter Clark, and Ashwin Kalyan. Learn to explain: Multimodal reasoning via thought chains for science question answering. *Advances in Neural Information Processing Systems*, 35: 2507–2521, 2022.

[37] Gen Luo, Yiyi Zhou, Yuxin Zhang, Xiawu Zheng, Xiaoshuai Sun, and Rongrong Ji. Feast your eyes: Mixture-of-resolution adaptation for multimodal large language models. *arXiv preprint arXiv:2403.03003*, 2024.

[38] Yulin Luo, Ruichuan An, Bocheng Zou, Yiming Tang, Jiaming Liu, and Shanghang Zhang. Llm as dataset analyst: Subpopulation structure discovery with large language model. In *European Conference on Computer Vision*, pages 235–252. Springer, 2025.

[39] Muhammad Maaz, Hanoona Rasheed, Salman Khan, and Fahad Shahbaz Khan. Video-chatgpt: Towards detailed video understanding via large vision and language models. *arXiv preprint arXiv:2306.05424*, 2023.

[40] Lingchen Meng, Hengduo Li, Bor-Chun Chen, Shiyi Lan, Zuxuan Wu, Yu-Gang Jiang, and Ser-Nam Lim. Adavit: Adaptive vision transformers for efficient image recognition. In *Proceedings of the IEEE/CVF Conference on Computer Vision and Pattern Recognition*, pages 12309–12318, 2022.

[41] Piotr Nawrot, Jan Chorowski, Adrian Łaćucki, and Edoardo M Ponti. Efficient transformers with dynamic token pooling. *arXiv preprint arXiv:2211.09761*, 2022.

[42] Maxime Oquab, Timothée Darcret, Théo Moutakanni, Huy Vo, Marc Szafraniec, Vasil Khalidov, Pierre Fernandez, Daniel Haziza, Francisco Massa, Alaaeldin El-Nouby, et al. Dinov2: Learning robust visual features without supervision. *arXiv preprint arXiv:2304.07193*, 2023.

[43] Long Ouyang, Jeffrey Wu, Xu Jiang, Diogo Almeida, Carroll Wainwright, Pamela Mishkin, Chong Zhang, Sandhini Agarwal, Katarina Slama, Alex Ray, et al. Training language models to follow instructions with human feedback. *Advances in neural information processing systems*, 35:27730–27744, 2022.

[44] Alec Radford, Jeffrey Wu, Rewon Child, David Luan, Dario Amodei, Ilya Sutskever, et al. Language models are unsupervised multitask learners. *OpenAI blog*, 1(8):9, 2019.

[45] Alec Radford, Jong Wook Kim, Chris Hallacy, Aditya Ramesh, Gabriel Goh, Sandhini Agarwal, Girish Sastry, Amanda Askell, Pamela Mishkin, Jack Clark, et al. Learning transferable visual models from natural language supervision. In *International conference on machine learning*, pages 8748–8763. PMLR, 2021.

[46] Jack W Rae, Anna Potapenko, Siddhant M Jayakumar, and Timothy P Lillicrap. Compressive transformers for long-range sequence modelling. *arXiv preprint arXiv:1911.05507*, 2019.

[47] Yongming Rao, Wenliang Zhao, Benlin Liu, Jiwen Lu, Jie Zhou, and Cho-Jui Hsieh. Dynamicvit: Efficient vision transformers with dynamic token sparsification. *Advances in neural information processing systems*, 34:13937–13949, 2021.

[48] Yuzhang Shang, Mu Cai, Bingxin Xu, Yong Jae Lee, and Yan Yan. Llava-prumerge: Adaptive token reduction for efficient large multimodal models. *arXiv preprint arXiv:2403.15388*, 2024.

[49] Noam Shazeer. Glu variants improve transformer. *arXiv preprint arXiv:2002.05202*, 2020.

[50] Amanpreet Singh, Vivek Natarajan, Meet Shah, Yu Jiang, Xinlei Chen, Dhruv Batra, Devi Parikh, and Marcus Rohrbach. Towards vqa models that can read. In *Proceedings of the IEEE/CVF conference on computer vision and pattern recognition*, pages 8317–8326, 2019.

[51] Gemini Team, Rohan Anil, Sébastien Borgeaud, Jean-Baptiste Alayrac, Jiahui Yu, Radu Soricut, Johan Schalkwyk, Andrew M Dai, Anja Hauth, Katie Millican, et al. Gemini: a family of highly capable multimodal models. *arXiv preprint arXiv:2312.11805*, 2023.

[52] Shengbang Tong, Zhuang Liu, Yuexiang Zhai, Yi Ma, Yann LeCun, and Saining Xie. Eyes wide shut? exploring the visual shortcomings of multimodal llms. In *Proceedings of the IEEE/CVF Conference on Computer Vision and Pattern Recognition*, pages 9568–9578, 2024.

[53] Hugo Touvron, Matthieu Cord, Matthijs Douze, Francisco Massa, Alexandre Sablayrolles, and Hervé Jégou. Training data-efficient image transformers & distillation through attention. In *International conference on machine learning*, pages 10347–10357. PMLR, 2021.

[54] Hugo Touvron, Thibaut Lavril, Gautier Izacard, Xavier Martinet, Marie-Anne Lachaux, Timothée Lacroix, Baptiste Rozière, Naman Goyal, Eric Hambro, Faisal Azhar, et al. Llama: Open and efficient foundation language models. *arXiv preprint arXiv:2302.13971*, 2023.

[55] Hugo Touvron, Louis Martin, Kevin Stone, Peter Albert, Amjad Almahairi, Yasmine Babaei, Nikolay Bashlykov, Soumya Batra, Prajwal Bhargava, Shruti Bhosale, et al. Llama 2: Open foundation and fine-tuned chat models. *arXiv preprint arXiv:2307.09288*, 2023.

[56] A Vaswani. Attention is all you need. *Advances in Neural Information Processing Systems*, 2017.

[57] Dejing Xu, Zhou Zhao, Jun Xiao, Fei Wu, Hanwang Zhang, Xiangnan He, and Yuetong Zhuang. Video question answering via gradually refined attention over appearance and motion. In *Proceedings of the 25th ACM international conference on Multimedia*, pages 1645–1653, 2017.

[58] Jun Xu, Tao Mei, Ting Yao, and Yong Rui. Msr-vtt: A large video description dataset for bridging video and language. In *Proceedings of the IEEE conference on computer vision and pattern recognition*, pages 5288–5296, 2016.

[59] Ruyi Xu, Yuan Yao, Zonghao Guo, Junbo Cui, Zanlin Ni, Chunjiang Ge, Tat-Seng Chua, Zhiyuan Liu, Maosong Sun, and Gao Huang. Llava-uhd: an lmm perceiving any aspect ratio and high-resolution images. *arXiv preprint arXiv:2403.11703*, 2024.

[60] Deming Ye, Yankai Lin, Yufei Huang, and Maosong Sun. Tr-bert: Dynamic token reduction for accelerating bert inference. *arXiv preprint arXiv:2105.11618*, 2021.

- [61] Weihao Ye, Qiong Wu, Wenhao Lin, and Yiyi Zhou. Fit and prune: Fast and training-free visual token pruning for multi-modal large language models. *arXiv preprint arXiv:2409.10197*, 2024.
- [62] Weihao Yu, Zhengyuan Yang, Linjie Li, Jianfeng Wang, Kevin Lin, Zicheng Liu, Xinchao Wang, and Lijuan Wang. Mm-vet: Evaluating large multimodal models for integrated capabilities. *arXiv preprint arXiv:2308.02490*, 2023.
- [63] Zhou Yu, Dejing Xu, Jun Yu, Ting Yu, Zhou Zhao, Yueteng Zhuang, and Dacheng Tao. Activitynet-qa: A dataset for understanding complex web videos via question answering. In *Proceedings of the AAAI Conference on Artificial Intelligence*, pages 9127–9134, 2019.
- [64] Susan Zhang, Stephen Roller, Naman Goyal, Mikel Artetxe, Moya Chen, Shuohui Chen, Christopher Dewan, Mona Diab, Xian Li, Xi Victoria Lin, et al. Opt: Open pre-trained transformer language models. *arXiv preprint arXiv:2205.01068*, 2022.
- [65] Yuan Zhang, Chun-Kai Fan, Junpeng Ma, Wenzhao Zheng, Tao Huang, Kuan Cheng, Denis Gudovskiy, Tomoyuki Okuno, Yohei Nakata, Kurt Keutzer, et al. Sparsevlm: Visual token sparsification for efficient vision-language model inference. *arXiv preprint arXiv:2410.04417*, 2024.

[CLS] Attention is All You Need for Training-Free Visual Token Pruning: Make VLM Inference Faster

Appendix

In this appendix, we first provide the details of the experimental setup in Appendix A, including information about the datasets, model architectures, and comparison methods. Then, in Appendix B, we offer a more detailed analysis of the attention in VLMs, along with more visualizations and insights. In Appendix C, we present additional experimental results, including results with richer details across different model architectures and visualizations of the ablation studies. Finally, Appendix D includes further efficiency analysis with FlashAttention.

A Details of Experimental Setup

A.1 Datasets

We evaluate our method on a total of 14 widely used benchmarks, including 10 image benchmarks and 4 video benchmarks. Each task is described as follows.

A.1.1 Image Benchmarks

We conduct experiments on 10 image benchmarks used in LLaVA [34], including 5 visual question answering benchmarks and 5 multi-modal reasoning benchmarks. All inference settings and evaluation metrics for these tasks follow the original configurations in LLaVA-1.5 [34].

VQAv2 [15]. The VQAv2 benchmark evaluates the model’s visual recognition capabilities through open-ended questions. It consists of 265,016 images from MSCOCO dataset [31], with each image containing at least 3 questions. The dataset incorporates adversarially balanced question design, ensuring that each question corresponds to at least two images with completely different answers, preventing models from relying solely on statistical patterns to derive answers. We utilize the LLaVA subset of test-dev set for evaluation, which includes 107,394 image-question pairs. Each question is associated with 10 ground truth answers, and automatic evaluation metrics are used for scoring.

GQA [20]. The GQA benchmark focuses on evaluating structured understanding and reasoning abilities for scenes depicted in images. In addition to images and questions, it provides scene graph annotations derived from the Visual Genome dataset [24] for each image, including structured descriptions of objects, attributes, and their relationships within the scene. The questions are generated using the scene graphs, ensuring that each question corresponds to a clear semantic path. We use the accuracy on the test-dev set for evaluation, which contains 12,578 image-question pairs.

VizWiz [16]. The VizWiz benchmark uses images captured by blind users to evaluate the model’s visual understanding capabilities in real-world scenarios. Each image is first taken and uploaded by a blind user, accompanied by a question. The question is then paired with 10 crowdsourced answers for automated evaluation. Since the images are captured by blind users in real-life settings, some questions may be difficult to answer due to issues like blur or poor lighting. Additionally, since the images and questions originate from the same source, some questions may not be directly relevant to the image. We evaluate the model using the test-dev set, which includes 8,000 image-question pairs.

ScienceQA [36]. The ScienceQA benchmark uses multiple-choice questions to evaluate the model’s zero-shot generalization on scientific topics. The dataset contains rich domain diversity across three subjects: natural sciences, language science, and social science. Questions within each subject are hierarchically organized by topic, category, and skill, encompassing a total of 26 topics, 127 categories, and 379 skills. The images are illustrations related to the questions, and some questions do not have corresponding images. We evaluate the model using a subset of the test set that includes both questions and images, referred to as SQA-IMG, which contains 2,017 image-question pairs.

TextVQA [50]. The TextVQA benchmark is designed to evaluate the model’s ability to recognize textual information within images, emphasizing the integration of optical character recognition (OCR) and natural language understanding. The images are primarily sourced from the Open Images v3 dataset [23] and contain a variety of scenarios such as signs, billboards, and product packaging that

contain rich text information. In addition to raw images, reference OCR tokens are also provided. Answers to the questions may be directly derived from the text in the images or require contextual reasoning. We evaluate the performance on a validation set containing 5,000 image-question pairs.

POPE [29]. The POPE benchmark evaluates the hallucination in large vision-language models through questions about object presence. The images are sourced from the MSCOCO dataset [31], and the questions focus on whether a specific object is present in the image, assessing the degree of object hallucination. We use the average F1 score across three different sampling strategies in the test set for evaluation, including 8,910 image-question pairs.

MME [14]. The MME benchmark aims to comprehensively evaluate the perceptual and cognitive capabilities of multi-modal models, encompassing a total of 14 subtasks. The perception tasks include OCR as well as coarse- and fine-grained recognition. Coarse-grained recognition primarily focuses on the presence, count, position, and color of objects, while fine-grained recognition involves identifying specific posters, celebrities, scenes, landmarks, and artworks. All questions are binary judgment tasks. We use the perception score for performance evaluation, with 2,374 image-question pairs in total.

MMBench [35]. The MMBench benchmark is designed to comprehensively evaluate the capabilities of multi-modal models. It defines three levels of competence from the top down, with the first level containing two basic abilities, perception and reasoning, the second level containing 6 more specific capabilities, and the third level containing 20 concrete tasks. Each task contains multiple choice questions to assess model performance on the task. The benchmark is available in both English and Chinese. The English version includes 4,377 image-question pairs, while the Chinese version, also referred to as **MMBench-CN**, contains 4,329 pairs. Both versions are used for evaluation.

MM-Vet [62]. The MM-Vet benchmark focuses on the integration of different core vision-language capabilities. It defines 6 core capabilities, including recognition, OCR, knowledge, language generation, spatial awareness, and mathematics, which are combined into 16 specific tasks. The benchmark utilizes ChatGPT assistant for evaluation, providing unified metrics for assessing answers of varying styles. It includes a total of 218 image-question pairs.

A.1.2 Video Benchmarks

To evaluate the performance of different methods in scenarios with higher visual redundancy, we also conduct experiments on 4 video benchmarks used in Video-LLaVA [30]. The evaluation follows Video-ChatGPT [39], using *gpt-3.5-turbo* assistant for scoring. Due to the commercial API usage limits, we follow [8] to use the first 1K samples of each benchmark in the experiments.

TGIF-QA [21]. The TGIF-QA benchmark extends image-based VQA tasks to videos, requiring models to focus on both spatial and temporal attentions. It includes 72K animated GIFs from the Tumblr GIF dataset [28] and 165K crowdsourced question-answer pairs. We evaluate model performance using the Frame QA task in this benchmark.

MSVD-QA [57]. The MSVD-QA benchmark is based on the Microsoft Research Video Description Corpus [6], which is commonly used for video captioning tasks. The question-answer pairs in the benchmark are derived from the descriptions in the corpus. The benchmark consists of 1,970 video clips and 50.5K question-answer pairs in total.

MSRVTT-QA [57]. The MSRVTT-QA benchmark is based on the Microsoft Research Video to Text dataset [58], which is larger and has more complex scenes than the MSVD dataset. The benchmark consists of 10K video clips and 243K question-answer pairs in total.

ActivityNet-QA [63]. The ActivityNet-QA benchmark is based on the ActivityNet dataset [4], consisting of 5,800 complex web videos with an average length of 180 seconds. The benchmark includes 58K question-answer pairs, all of which are manually annotated to ensure higher quality.

A.2 Model Architectures

LLaVA-1.5 [32]. LLaVA is one of the most widely used open-source vision-language models, and its simple design, low tuning cost, and outstanding performance make it a cornerstone in the field of multi-modal models. Specifically, LLaVA employs a pre-trained CLIP as the visual encoder and Vicuna as the text decoder. A simple linear projector connects the two modules, enabling the LLM to accept visual tokens of CLIP as input. Meanwhile, visual instruction tuning allows the model to

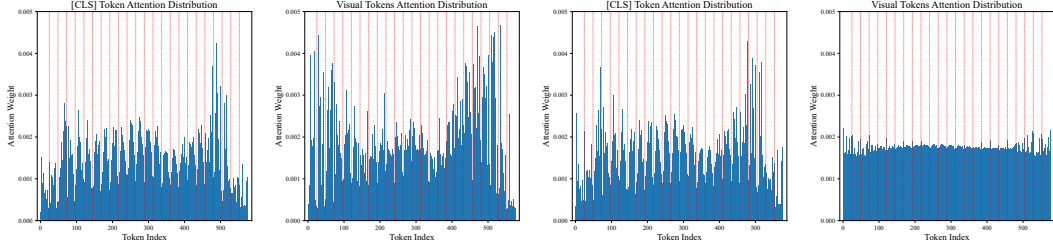


Figure 6: Distribution of visual attention over token positions in CLIP. From left to right: attention distribution of the [CLS] token in the penultimate layer, average attention distribution across all visual tokens in the penultimate layer, attention distribution of the [CLS] token in the final layer, and average attention distribution across all visual tokens in the final layer. The red vertical dashed lines indicate the length of each row in the input image (24 for CLIP-ViT-L-14-336px used in LLaVA-1.5).

handle vision-language tasks. Compared to the original LLaVA, LLaVA-1.5 increases the input image resolution from 224 to 336 and incorporates more instruction tuning data, resulting in a significant performance improvement.

LLaVA-NeXT [33]. Also known as LLaVA-1.6, LLaVA-NeXT builds upon LLaVA-1.5 by further increasing the input image resolution, achieving improvements in reasoning, OCR, and world knowledge. Unlike the fixed resolution increase in LLaVA-1.5, LLaVA-NeXT employs a dynamic high-resolution design. Specifically, the model can select the best aspect ratio based on the resolution of the input image, increasing the resolution by up to 4x. Without altering the visual encoder, high-resolution images are split into several sub-images of the same size as the original image. These sub-images are individually encoded and concatenated before being fed into the LLM.

Video-LLaVA [30]. On the basis of image understanding, Video-LLaVA extends this capability to video comprehension. It unifies representations of images and videos through alignment before projection. The overall architecture remains consistent with LLaVA: the visual encoder encodes continuous video frames individually, and the representations are concatenated as inputs to the LLM. After joint training, Video-LLaVA is capable of understanding both image and video data.

A.3 Comparison Methods

FastV [8]. In vision-language models, visual tokens contribute significantly to computational overhead. FastV first identifies the inefficient visual attention phenomena in VLMs and proposes a straightforward method to address this. Specifically, it prunes visual tokens with the lowest R% visual-text attention scores after layer 2 of the LLM, according to specific computation budget constraints, thereby accelerating VLM inference.

FitPrune [61]. Based on FastV, FitPrune investigates when and how to prune visual tokens more effectively. It uses binary search to keep the distribution of visual-text attention as unchanged as possible under given computational constraints, resulting in an optimal pruning strategy. Then, visual tokens are pruned according to the pre-calculated strategy, maximizing the preservation of original performance.

SparseVLM [65]. Unlike previous approaches, SparseVLM focuses on the influence of text prompts on visual-text attention. It proposes that not all text information is beneficial for pruning visual tokens. SparseVLM first selects text tokens relevant to the visual input and uses these raters to guide the pruning of visual tokens. Additionally, it employs a token recycle mechanism to retain more critical information, achieving notable performance improvements.

B Detailed Analysis of Attention in VLMs

B.1 Attention distribution

We first present the distribution of visual attention in CLIP. As shown in Fig. 6, the left two subplots show the visual attention in the penultimate layer of CLIP. The visual tokens used in LLaVA-1.5 also

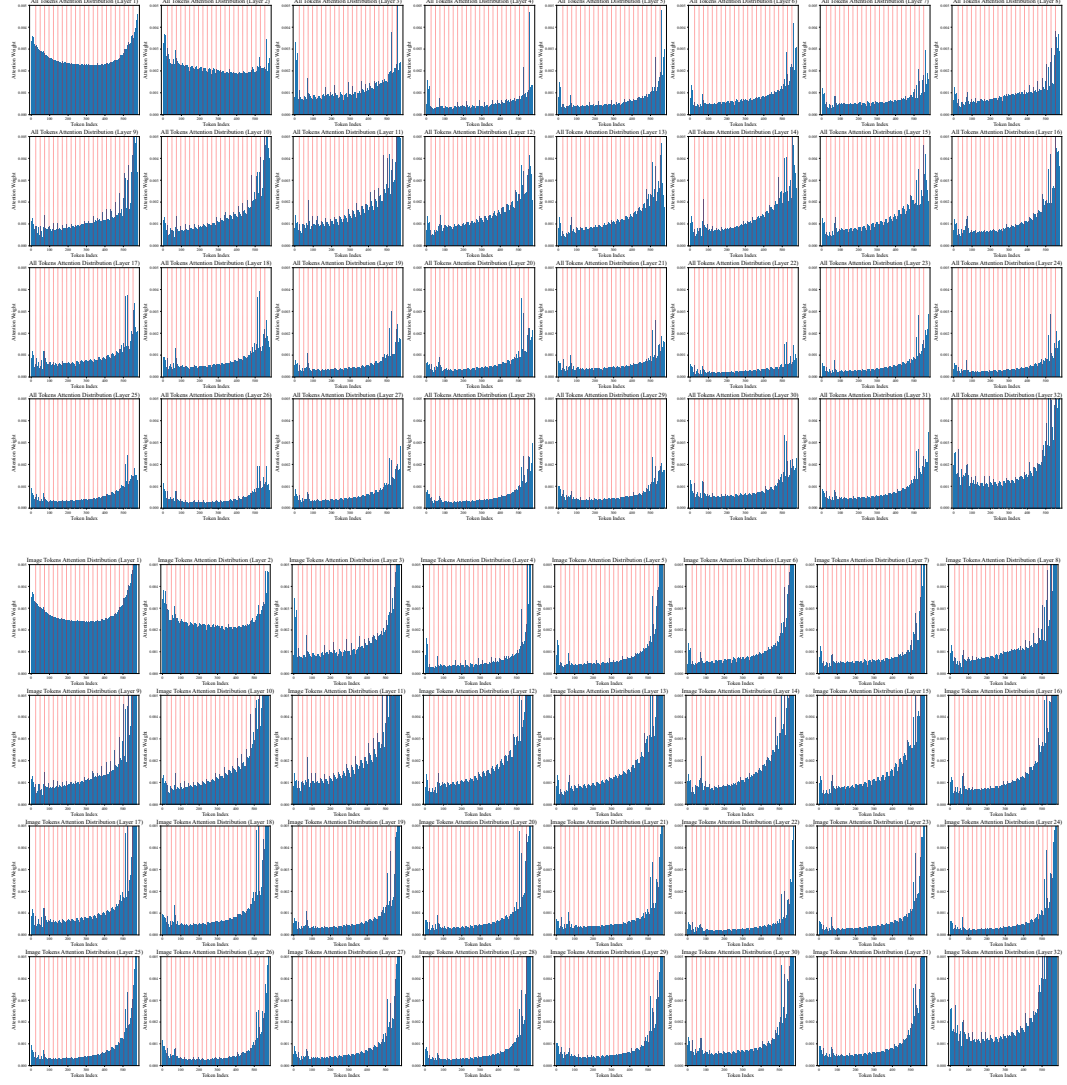


Figure 7: Distribution of visual-text attention over visual token positions in LLaMA. The top rows display the average attention distribution across all tokens, while the bottom rows display the attention distribution from other visual tokens. Each type of attentions include results from all 32 layers of the 7B language model. The red vertical dashed lines indicate the length of each row in the input image (24 for CLIP-ViT-L-14-336px used in LLaVA-1.5).

come from this layer, which retains more local features and image details. The right two subplots show the visual attention in the final layer of CLIP, which serves as the output layer. In the penultimate layer, attention from the [CLS] token is more concentrated compared to attention from other visual tokens, primarily focusing on regions closer to the image center. The [CLS] attention in the final layer is similar to that in the penultimate layer, but attention from other visual tokens becomes uniformly distributed due to the lack of supervision signals. Based on these observations, we adopt the [CLS] attention from the penultimate layer for visual token pruning.

Fig. 7 and Fig. 8 show the distribution of visual-text attention in the 32 layers of the 7B LLaMA language model, focusing on attention from all tokens, other visual tokens, language instruction tokens, and the last token. Unlike the attention distributions in the visual encoder, these visual-text attention distributions exhibit a clear trend of increasing intensity with larger token indices, which termed *attention shift* in the main text. Pruning visual tokens based on such attention leads to significant performance degradation, especially at high reduction ratios. This shift phenomenon is

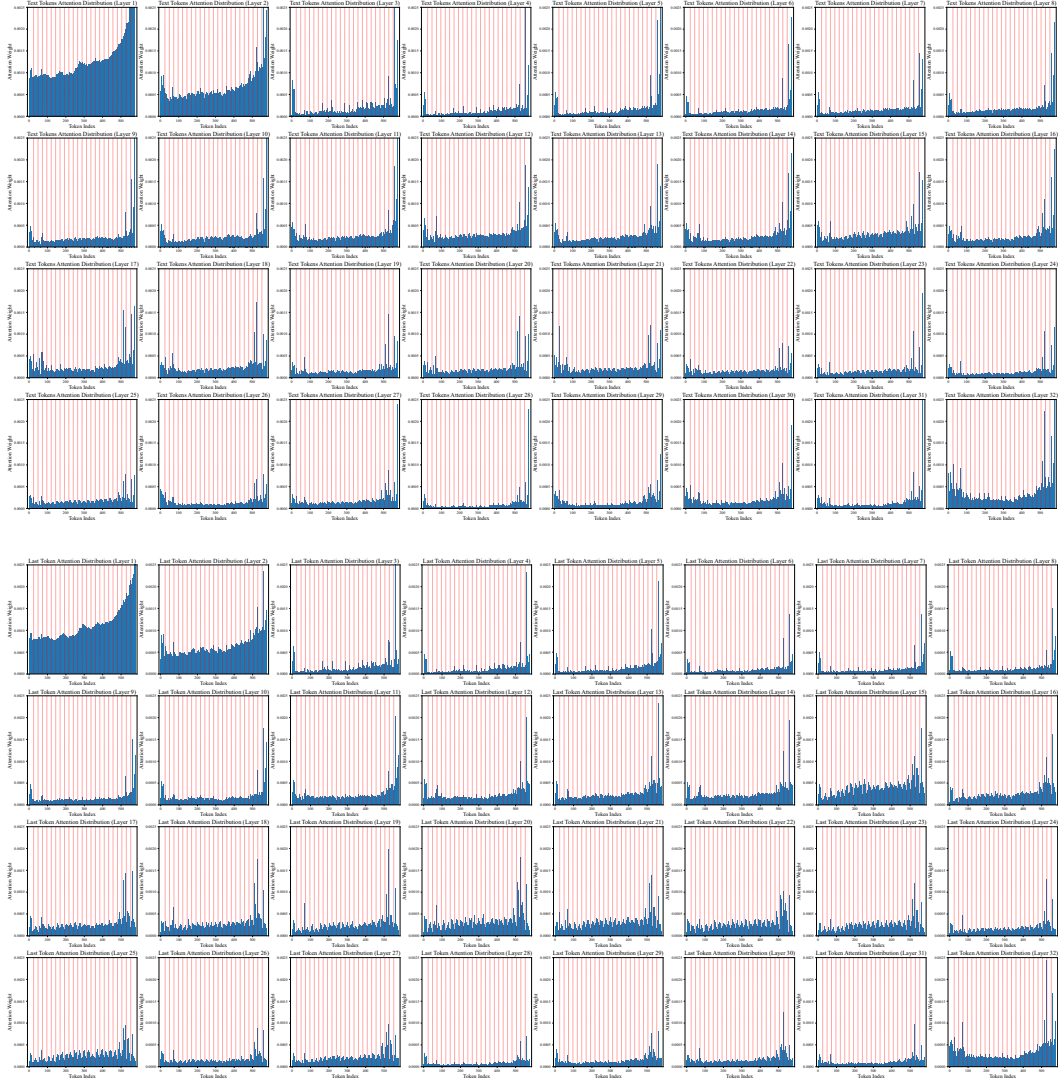


Figure 8: Distribution of visual-text attention over visual token positions in LLaMA. The top rows display the attention distribution from language instruction tokens, while the bottom rows display the attention distribution of the last token, which is also used to predict the next token. Each type of attentions include results from all 32 layers of the 7B language model. The red vertical dashed lines indicate the length of each row in the input image (24 for CLIP-ViT-L-14-336px used in LLaVA-1.5).

consistently observed across all types of visual-text attention. Notably, attention from the text tokens is significantly weaker than from the visual part, especially after the second layer, corroborating the inefficient visual attention phenomenon identified in FastV [8] and providing sufficient motivation for visual token pruning. Additionally, we observe that the attention distribution in the first 2 layers differs noticeably from the subsequent 30 layers. Deeper analysis of this distinction and how to leverage it to improve VLM performance is left as future work.

B.2 Attention intensity

We visualize the attention maps from the [CLS] token in the visual encoder and the last token in the language model for the same input images in Fig. 9. The attention from the [CLS] token is more concentrated, focusing on key foreground objects like Big Ben, train carriages, paragliders, sticky notes, the bird, giraffes, and the titles on book covers, as well as certain artifacts that encode

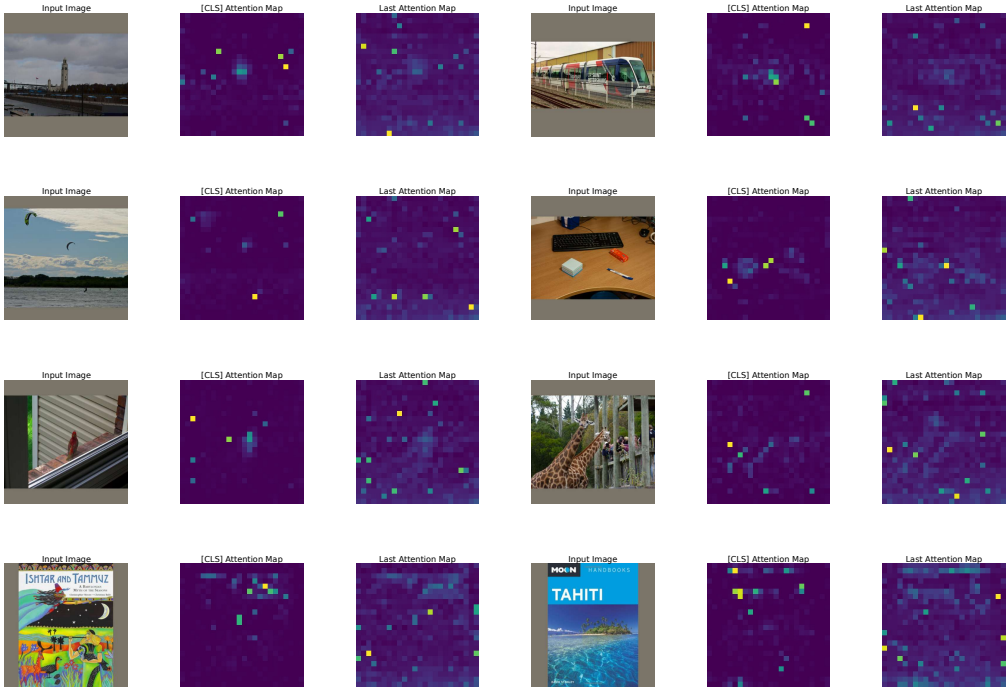


Figure 9: Visualizations of attention maps from the [CLS] token in the visual encoder and the last token in the language model. The attention in the visual encoder is concentrated, with higher attention to key foreground objects and regions that aggregate global information, while other areas receive little attention. In contrast, the attention in the language model is more dispersed and contains more noise, with important visual tokens receiving less attention. The highest attention tends to focus on the padding region, and attention is stronger in the lower part of the image than in the upper part.

global information. In contrast, the attention from the last token in the language model is more dispersed, spread across the entire input image. This indicates that it includes more noise, making it less effective for accurately evaluating the importance of visual tokens. This discrepancy highlights a degree of misalignment between the visual and language modalities in existing vision-language models. Addressing this misalignment to improve VLM performance on multi-modal understanding tasks remains a direction for future work.

C Additional Experimental Results

We provide further results for different methods on LLaVA-1.5-7B, LLaVA-1.5-13B, LLaVA-NeXT-7B, and Video-LLaVA in Tab. 7, Tab. 8, Tab. 9, and Tab. 10. Notably, the pruning scheme fitting algorithm of FitPrune is not compatible with the larger 13B language model or LLaVA-NeXT with dynamic number of visual tokens. Additionally, SparseVLM cannot reduce the number of visual tokens below 95% due to its pruned token recycling design. Our method achieves outstanding performance across all model architectures and different reduction ratios, demonstrating its simplicity and effectiveness. Notably, compared to the 7B version of LLaVA-1.5, increasing the size of the language model improves the performance of VLM on multi-modal tasks. Further improvements can be achieved with higher resolution image inputs. With just the 7B language model, LLaVA-NeXT outperforms LLaVA-1.5, which uses the 13B language model. Additionally, video inputs, which contain more redundancy than single images, benefit more from visual token pruning.

Fig. 10 visualizes the performance of FasterVLM on LLaVA-1.5-7B across different reduction ratios. Our method maintains strong performance even at a 95% reduction ratio, significantly outperforming versions that do not use visual input. This demonstrates the critical importance of a small number of key visual tokens in VLM performance. Fig. 11 presents the results of ablation experiments on

Table 7: Performance comparison of different methods with LLaVA-1.5-7B across 10 benchmarks under varying reduction ratios. For each reduction ratio, the best average performance is shown in **bold**, and the second best one is underlined. 100% reduction ratio represents using no input images.

Method	Reduction Ratio	# Token	VQAv2	GQA	VizWiz	SQA-IMG	TextVQA	POPE	MME	MMB	MMB-CN	MM-Vet	Average
LLaVA-1.5-7B	0%	576	78.52	61.94	50.06	69.51	58.21	85.88	1506.47	64.69	58.08	31.30	100.00%
FastV	25%	432	78.45	61.69	50.30	69.31	58.09	85.29	1528.16	64.52	58.76	32.80	100.60%
FitPrune			78.49	61.93	50.07	69.51	58.27	85.94	1512.72	64.60	58.33	31.50	100.15%
SparseVLM			78.13	61.38	50.38	68.62	57.44	84.56	1475.47	64.78	57.30	32.40	99.54%
FasterVLM			78.39	61.51	50.01	68.57	57.91	85.92	1501.10	65.12	58.51	32.40	100.18%
FastV	50%	288	77.67	60.05	50.53	68.96	58.25	82.45	1513.06	64.26	58.16	31.70	99.33%
FitPrune			78.41	61.70	50.04	69.16	58.26	85.37	1499.70	64.60	58.16	31.10	99.73%
SparseVLM			76.67	58.78	51.03	68.57	57.49	83.87	1458.79	63.14	56.87	31.50	98.52%
FasterVLM			77.86	60.64	50.45	68.37	57.90	86.20	1471.96	63.83	56.70	34.80	100.12%
FastV	75%	144	74.07	56.58	51.29	69.11	57.38	73.74	1463.39	64.00	57.22	28.60	95.80%
FitPrune			76.14	59.38	51.30	69.01	56.49	80.75	1472.86	63.92	57.65	28.40	97.22%
SparseVLM			72.76	55.11	51.46	69.36	55.99	77.57	1351.65	59.54	51.03	29.90	93.84%
FasterVLM			76.19	58.34	51.97	67.92	57.07	83.46	1433.76	62.54	57.13	34.20	98.75%
FastV	90%	58	65.38	51.20	51.84	69.81	54.75	57.30	1210.36	59.97	51.72	27.20	87.97%
FitPrune			62.76	49.96	50.85	68.22	50.35	53.81	1147.46	56.27	45.53	21.80	82.07%
SparseVLM			62.90	48.86	49.36	67.23	48.99	65.82	1030.61	49.05	35.40	18.60	78.13%
FasterVLM			71.92	54.91	53.01	68.91	55.28	75.85	1348.63	60.57	54.90	30.10	94.24%
FastV	95%	29	55.92	46.03	49.10	70.00	51.56	35.47	971.56	50.17	42.18	18.90	74.93%
FitPrune			52.39	43.60	48.61	68.32	46.75	31.17	855.21	39.69	29.98	18.00	67.64%
FasterVLM			66.75	51.51	52.67	69.56	53.09	67.24	1254.80	58.51	51.98	27.50	89.41%
LLaVA-1.5-7B	100%	0	40.73	37.38	45.36	63.06	41.43	47.21	719.10	20.02	17.70	11.30	56.50%

Table 8: Performance comparison of different methods with LLaVA-1.5-13B across 10 benchmarks under varying reduction ratios. For each reduction ratio, the best average performance is shown in **bold**, and the second best one is underlined. 100% reduction ratio represents using no input images.

Method	Reduction Ratio	# Token	VQAv2	GQA	VizWiz	SQA-IMG	TextVQA	POPE	MME	MMB	MMB-CN	MM-Vet	Average
LLaVA-1.5-13B	0%	576	80.00	63.25	53.61	72.78	61.19	85.99	1531.19	68.47	63.49	36.30	100.00%
FastV	25%	432	79.96	63.11	53.79	72.78	61.29	85.86	1543.97	68.38	63.40	35.20	99.76%
SparseVLM			79.25	61.29	53.60	73.77	60.46	72.45	1481.40	68.30	61.77	35.50	97.20%
FasterVLM			79.61	61.24	53.16	72.98	60.35	86.73	1487.34	67.61	63.40	36.70	99.21%
FastV			78.54	62.59	54.34	73.13	60.86	85.15	1545.14	68.47	63.23	34.80	99.51%
SparseVLM	50%	288	78.48	59.90	53.08	74.02	59.48	71.30	1497.39	66.67	61.94	36.50	96.69%
FasterVLM			79.03	61.01	52.65	73.62	59.99	86.05	1530.41	67.70	62.80	36.80	99.18%
FastV	75%	144	77.24	59.87	54.82	74.02	60.07	79.43	1495.51	67.27	62.63	33.20	97.16%
SparseVLM			76.06	57.97	53.13	73.67	57.94	68.61	1499.49	64.52	59.11	35.00	94.32%
FasterVLM			77.36	58.74	52.74	73.48	58.99	83.10	1467.00	67.10	62.54	36.30	97.43%
FastV	90%	58	70.27	54.92	54.78	72.43	55.64	67.26	1359.69	63.83	59.71	29.40	90.26%
SparseVLM			68.27	54.43	50.45	70.35	52.56	62.63	1285.26	58.16	54.30	27.20	85.02%
FasterVLM			73.08	55.98	54.00	73.72	57.35	74.71	1370.77	65.21	61.08	33.90	93.68%
FastV	95%	29	62.25	50.34	52.96	73.18	52.08	49.83	1165.70	56.44	51.29	24.00	80.53%
FasterVLM			67.85	52.62	53.11	72.83	54.82	65.90	1267.09	62.11	56.87	31.60	88.35%
LLaVA-1.5-13B	100%	0	41.40	38.40	45.15	66.63	43.51	1.45	622.91	22.77	18.13	13.20	49.99%

various pruning strategies. By performing visual token pruning based on the [CLS] attention before LLM, our FasterVLM achieves remarkable efficiency. This design, while simple, proves to be highly effective in preserving model performance while reducing computational complexity.

D Efficiency Analysis with FlashAttention

In Tab. 11, Tab. 12 and Tab. 13, we compare the computational efficiency between FastV and our FasterVLM under LLaVA-1.5-7B, LLaVA-1.5-13B, and LLaVA-NeXT-7B, respectively. Unlike FastV, which prune visual token within the LLM, FasterVLM prunes tokens before the LLM, enabling compatibility with FlashAttention. This design results in significantly higher efficiency. Note that the original implementation of SDPA also includes FlashAttention, so its computational efficiency is comparable to that of FlashAttention2, with only slight differences. All efficiency analyses are performed on a single NVIDIA A100-80GB GPU, evaluated using the POPE benchmark.

Table 9: Performance comparison of different methods with LLaVA-NeXT-7B across 10 benchmarks under varying reduction ratios. For each reduction ratio, the best average performance is shown in **bold**, and the second best one is underlined. 100% reduction ratio represents using no input images.

Method	Reduction Ratio	# Token	VQAv2	GQA	VizWiz	SQA-IMG	TextVQA	POPE	MME	MMB	MMB-CN	MM-Vet	Average
LLaVA-NeXT-7B	0%	2880	81.21	62.93	55.21	69.66	59.59	86.32	1513.78	67.70	58.85	42.60	100.00%
FastV	25%	2160	81.12	62.50	55.05	69.31	59.69	86.27	1506.28	67.61	59.02	41.70	99.61%
SparseVLM	25%	2160	81.14	62.55	55.20	68.47	60.26	73.15	1507.75	66.07	58.59	41.90	97.86%
FasterVLM			81.18	62.81	56.12	70.70	59.65	86.26	1492.20	67.35	58.33	44.30	100.41%
FastV	50%	1440	80.71	61.76	54.89	69.06	59.55	85.46	1490.34	67.35	58.51	41.20	98.91%
SparseVLM	50%	1440	80.92	62.04	55.71	68.07	60.00	73.42	1484.92	65.72	58.85	39.90	97.14%
FasterVLM			80.72	62.66	55.82	69.41	59.72	86.66	1521.87	67.87	58.85	44.40	100.53%
FastV	75%	720	78.90	60.38	54.22	69.81	58.39	83.09	1477.31	65.64	57.04	41.10	97.37%
SparseVLM	75%	720	78.86	60.88	55.55	67.48	58.08	70.99	1446.10	63.83	57.04	38.00	94.95%
FasterVLM			79.25	61.31	56.24	68.82	59.33	85.50	1480.68	67.53	59.19	40.40	98.73%
FastV	90%	288	71.94	55.86	53.07	69.26	55.69	71.66	1282.86	61.60	51.89	33.70	89.24%
SparseVLM	90%	288	71.62	56.12	53.16	68.62	51.97	63.23	1332.22	54.47	50.69	24.70	84.52%
FasterVLM			75.21	58.12	56.92	68.12	57.57	80.00	1370.11	63.32	54.47	35.70	93.55%
FastV	95%	144	61.84	49.83	51.25	68.52	51.85	51.66	1079.46	54.90	45.36	21.90	77.43%
FasterVLM	95%	144	70.63	54.73	56.27	68.86	55.97	72.89	1225.96	60.48	53.09	31.90	88.85%
LLaVA-NeXT-7B	100%	0	40.59	37.93	46.01	64.01	37.57	23.40	601.93	21.05	17.70	13.10	50.73%

Table 10: Performance comparison of different methods with Video-LLaVA across 4 video question answering benchmarks under varying reduction ratios. Evaluation was performed using the first 1,000 samples from each benchmark with *gpt-3.5-turbo* assistant. For each reduction ratio, the best average performance is highlighted in **bold**, and 100% reduction ratio represents using no video frames.

Method	Reduction Ratio	# Token	TGIF-QA Acc.	TGIF-QA Score	MSVD-QA Acc.	MSVD-QA Score	MSRVTT-QA Acc.	MSRVTT-QA Score	ActivityNet-QA Acc.	ActivityNet-QA Score	Average Acc.	Average Score
Video-LLaVA	0%	2048	19.80	2.53	70.50	3.93	57.50	3.50	43.60	3.81	100.00%	100.00%
FastV	25%	1536	19.60 19.80	2.54 2.53	70.50 72.00	3.94 3.96	55.40 57.10	3.47 3.48	44.20 45.00	3.86 3.88	99.18% 101.16%	100.24% 100.45%
FasterVLM	50%	1024	19.50 19.20	2.54 2.51	70.40 71.90	3.94 3.96	54.80 56.70	3.46 3.47	43.40 44.90	3.81 3.87	98.30% 100.14%	99.79% 100.11%
FasterVLM			19.40 17.90	2.51 2.48	69.10 70.20	3.91 3.95	54.60 56.60	3.43 3.50	41.50 44.70	3.80 3.86	96.53% 97.73%	99.12% 99.88%
FastV	75%	512	13.80 15.60	2.40 2.39	68.80 69.10	3.90 3.92	52.90 55.30	3.40 3.43	41.30 44.50	3.79 3.82	88.50% 93.76%	97.63% 98.04%
FasterVLM	90%	208	10.60 14.00	2.29 2.34	64.10 65.30	3.78 3.79	52.40 53.80	3.39 3.40	40.30 43.70	3.78 3.79	82.00% 89.28%	95.64% 96.37%
FasterVLM			14.00	2.34	65.30	3.79	53.80	3.40	43.70	3.79	89.28%	96.37%
Video-LLaVA	100%	0	5.70	1.96	23.40	1.77	24.50	1.87	39.10	3.66	48.57%	68.01%

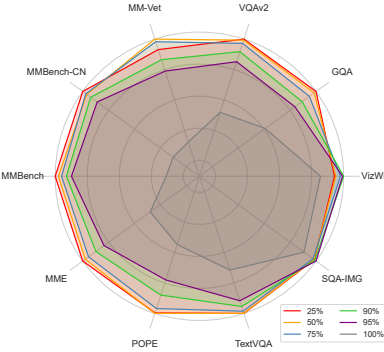


Figure 10: Performance of FasterVLM on LLaVA-1.5-7B across 10 benchmarks at varying reduction ratios from 25% to 100%.

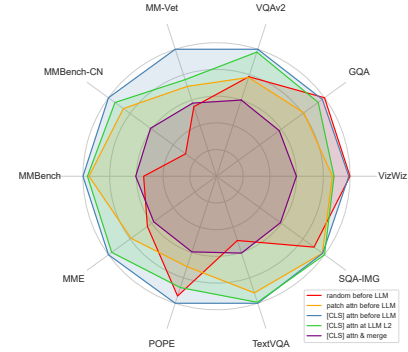


Figure 11: Ablation study on different pruning strategies in FasterVLM, showing performance across 10 benchmarks.

Table 11: Efficiency comparison between FastV and FasterVLM under LLaVA-1.5-7B.

Method	Reduction	# Token	FLOPs (T)	Storage (MB)	GPU Memory (GB)	CUDA Time (ms)	Accuracy (%)
LLaVA-1.5-7B	0%	576	8.02	288.00	14.68	107.26	85.88
FastV				6.20	220.50	107.09	85.29
FasterVLM (sdpa)	25%	432	6.08	216.00	14.51	101.95	85.92
FasterVLM (flash attention)						101.35	85.87
FastV	50%	288	4.40	153.00	14.52	99.72	82.45
FasterVLM (sdpa)			4.16	144.00	14.46	93.57	86.20
FasterVLM (flash attention)						92.26	86.16
FastV	75%	144	2.62	85.50	14.52	94.67	73.74
FasterVLM (sdpa)			2.26	72.00	14.44	85.06	83.46
FasterVLM (flash attention)						84.03	83.42
FastV	90%	58	1.57	45.31	14.64	90.48	57.30
FasterVLM (sdpa)			1.13	29.00	14.54	79.11	75.85
FasterVLM (flash attention)						77.44	75.82
FastV	95%	29	1.22	31.72	14.63	89.31	35.47
FasterVLM (sdpa)			0.76	14.50	14.54	78.09	67.24
FasterVLM (flash attention)						77.15	67.22

Table 12: Efficiency comparison between FastV and FasterVLM under LLaVA-1.5-13B.

Method	Reduction	# Token	FLOPs (T)	Storage (MB)	GPU Memory (GB)	CUDA Time (ms)	Accuracy (%)
LLaVA-1.5-13B	15.28	450.00	26.98	156.64	85.99	107.26	85.88
FastV			11.69	343.13	26.61	151.66	85.86
FasterVLM (sdpa)	25%	432	11.50	337.50	26.58	138.36	86.73
FasterVLM (flash attention)						137.95	86.72
FastV	50%	288	8.14	236.25	26.40	137.83	85.15
FasterVLM (sdpa)			7.76	225.00	26.31	124.13	86.05
FasterVLM (flash attention)						123.33	86.04
FastV	75%	144	4.62	129.38	26.40	123.69	79.43
FasterVLM (sdpa)			4.05	112.50	26.29	104.81	83.10
FasterVLM (flash attention)						103.57	83.09
FastV	90%	58	2.53	65.70	26.40	114.98	67.26
FasterVLM (sdpa)			1.86	45.31	26.27	94.80	74.71
FasterVLM (flash attention)						94.04	74.66
FastV	95%	29	1.83	44.19	26.55	114.25	49.83
FasterVLM (sdpa)			1.12	22.66	26.43	94.48	65.90
FasterVLM (flash attention)						93.73	65.79

Table 13: Efficiency comparison between FastV and FasterVLM under LLaVA-NeXT-7B.

Method	Reduction	# Token	FLOPs (T)	Storage (MB)	GPU Memory (GB)	CUDA Time (ms)	Accuracy (%)
LLaVA-NeXT-7B	0%	2880	43.58	1440.00	17.04	313.04	86.77
FastV			33.05	1102.50	16.95	262.49	86.63
FasterVLM (sdpa)	25%	2160	32.35	1080.00	16.33	246.38	86.69
FasterVLM (flash attention)						232.07	86.66
FastV	50%	1440	23.04	765.00	16.95	201.68	85.73
FasterVLM (sdpa)			21.66	720.00	15.11	170.30	87.06
FasterVLM (flash attention)						147.93	87.02
FastV	75%	720	13.53	427.50	16.95	119.87	82.68
FasterVLM (sdpa)			11.51	360.00	14.80	116.79	86.50
FasterVLM (flash attention)						104.46	86.46
FastV	90%	290	8.10	226.56	16.95	117.33	70.77
FasterVLM (sdpa)			5.71	145.00	14.70	87.36	81.17
FasterVLM (flash attention)						85.26	81.12
FastV	95%	145	6.30	158.59	16.95	112.19	49.36
FasterVLM (sdpa)			3.80	72.50	14.70	78.18	74.77
FasterVLM (flash attention)						77.66	74.72